Low-temperature properties of the Yb-based heavy-fermion antiferromagnets YbPtIn, YbRhSn, and YbNiGa

O. Trovarelli, C. Geibel, R. Cardoso, S. Mederle, R. Borth, B. Buschinger, F. M. Grosche, Y. Grin, G. Sparn, and F. Steglich

Max-Planck-Institute for Chemical Physics of Solids, D-01187 Dresden, Germany

(Received 22 April 1999; revised manuscript received 10 December 1999)

The crystallographic and low-temperature properties of the equiatomic Yb-based compounds YbPtIn, YbRhSn (hexagonal ZrNiAl structure), and YbNiGa (orthorhombic ϵ-TiNiSi structure) are studied by means of x-ray diffraction, magnetic susceptibility, magnetization, electrical resistivity (ρ), magnetoresistance, thermoelectric power, and specific-heat (C_P) measurements. The magnetic susceptibility follows a Curie-Weiss law with effective magnetic moments close to the value of Yb^{3+} and shows strong magnetocrystalline anisotropy. At low temperature the three compounds exhibit the typical properties of antiferromagnetic (AFM) Kondo lattices, namely a logarithmic increase of $\rho(T)$, enhanced electronic C_P coefficients γ_o, and a reduced entropy gain below the ordering temperature. The values of $\gamma_o > 350$ mJ/mol K^2 are among the largest of known Yb-based magnetic Kondo lattices. Two AFM transitions in each compound evidence a competition between single-ion anisotropy and frustration of the magnetic interactions due to the topology of the underlying crystal structure. The ground-state properties are discussed and compared with those of other *f*-electron compounds showing similar characteristics concerning magnetic frustration.

I. INTRODUCTION

The study of magnetically ordered (MO) Kondo lattices (KL's) has become a topic of current interest in the physics of strongly correlated *f*-electron systems since the observation, in several Ce-based intermetallic compounds, of non-Fermi-liquid effects or the onset of superconductivity close to the phase transition between MO and nonmagnetic (NM) states.[1] Whereas the present knowledge about MO KL's has been achieved from thorough investigations performed mainly in Ce- and U-based compounds, considerably less information is available for MO KL based on ytterbium, because of the difficult task of the sample preparation.[2] Despite the hole-electron analogy between $4f^{13}$-Yb^{3+} and $4f^{1}$-Ce^{3+} electronic configurations gives the possibility of finding Yb compounds with similar properties as those based on Ce, most known Yb intermetallic compounds are found in a mixed-valent (MV) state. In comparison to Ce compounds relatively few Yb counterparts exhibit the archetypal properties of MO KL's or heavy fermions.[2–4] In these materials the interplay between MO and NM states is generally considered to depend on the competition between intrasite Kondo effect and intersite Ruderman-Kittel-Kasuya-Yosida (RKKY) interactions through the hybridization strength $\mathcal{J}$ between the *f* and the conduction electrons.[5] Thus for small $\mathcal{J}$ the RKKY interaction dominates and MO is expected at a temperature T_m. As $\mathcal{J}$ increases, the local moments are progressively screened by the Kondo effect and the enhanced density of electronic states at the Fermi energy leads to heavy-fermion behavior. Finally, for very strong hybridization a NM-MV ground state (GS) takes place. The transition between MO and NM states is expected at the critical value $\mathcal{J}_c$ where $T_m \simeq 0$. Although this model provides a qualitative description of the main features of Ce-based KL systems,[5] it is still not clear whether the same picture can be applied to Yb compounds because of the lack of examples in the vicinity of $\mathcal{J}_c$ at normal conditions.[2–4] In this paper we study three Yb-based compounds which are close to the magnetic side of $\mathcal{J}_c$ and therefore show the typical properties of heavy-fermion antiferromagnets: YbPtIn, YbRhSn, and YbNiGa.

The search and study of Yb-based ternary compounds with the composition *RTX* (*R*=Yb, *T*=transition metal, *X*=*p* element) currently attracts the interest of several research groups.[6–9] These compounds crystallize mainly in two structure types, i.e., in the orthorhombic ϵ-TiNiSi or in the hexagonal ZrNiAl type, which are ordered structures with

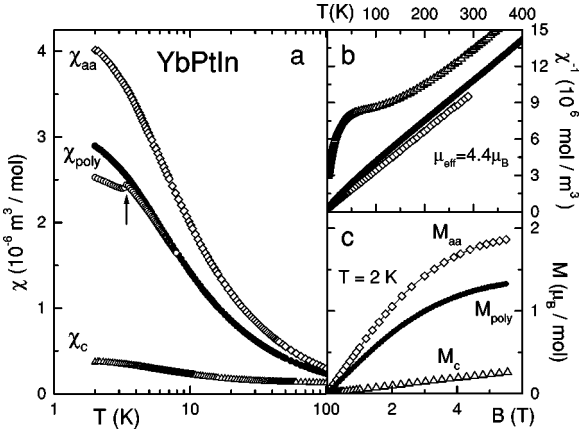

FIG. 1. (a) Magnetic susceptibility of YbPtIn, in a log-*T* scale, for random powder (χ_{poly}) measured in $B=0.01$ T (○) and $B=0.2$ T (●) as well as for a single crystal in $B=0.2$ T applied along the basal plane of the structure (χ_{aa}) and along the *c* axis (χ_c). The arrow indicates the magnetic transition at $T_{N1}=3.4$ K, observed at low magnetic fields only. (b) Inverse susceptibility of the data shown in (a). (c) Magnetization of single-crystalline YbPtIn at $T=2$ K measured along the basal plane (M_{aa}) and along the *c* axis (M_c). The isotherm on random powder (M_{poly}) is included for comparison.

TABLE I. Lattice parameters and unit-cell volume of YbPtIn and YbRhSn (hexagonal ZrNiAl-type structure, space group $P\bar{6}2m$) and of YbNiGa (orthorhombic ϵ-TiNiSi-type, space group $Pnma$), determined from x-ray powder-diffraction data using Si as internal standard.

	a [nm]	b [nm]	c [nm]	V [nm^3]
YbPtIn	0.7548(1)		0.3766(1)	0.1888(1)
YbRhSn	0.7531(3)		0.3666(6)	0.1801(2)
YbNiGa	0.6728(1)	0.4234(1)	0.7212(1)	0.2083(1)

only one equivalent crystallographic site for the R atoms.[10,11] One of the characteristics of these structures is that the crystalline-electric field (CEF) at the R site usually induces strong single-ion anisotropy.[12] In particular, the MO-KL compounds YbPtAl (Refs. 13 and 14) and YbNiSn (Ref. 15) (ϵ-TiNiSi structure), as well as YbNiAl (ZrNiAl structure),[13,16] have been intensively investigated due to their interesting magnetic properties. In the orthorhombic heavy-fermion ferromagnet YbNiSn strong single-ion anisotropy competes with the anisotropy of the magnetic exchange interaction between nearest- and next-nearest magnetic neighbors.[15] As a result, complex noncolinear spin structures with an unusual volume dependence of the ordering temperature have been observed as a function of hydrostatic pressure and ascribed to the interplay between strong magnetocrystalline anisotropy and frustrated anisotropic exchange interactions.[15] On the other hand, the hexagonal compound YbNiAl was recently reported as the first example of an Yb-based heavy-fermion antiferromagnet (AFM).[13] In this compound the Yb moments lie in the basal plane of the structure forming an ''easy-plane'' hexagonal array similar to a *kagomé* lattice and, in addition to strong single-ion anisotropy, AFM coupling between nearest neighbors leads to geometrical frustration.[16] Neutron-scattering experiments revealed a complex magnetic structure with nonordered moments lying between MO chains, characterized by an incommensurate propagation vector parallel to the hexagonal plane, in a substantially different situation to other members of the RTAl series, like CePdAl (Ref. 17) or TbNiAl,[18] which show ''easy-axis''-type frustrated structures. The Yb-based compounds further present the advantage of allowing a direct investigation at the Yb site by using Mössbauer spectroscopy as a local probe technique.[14,15]

In the compounds YbPtIn, YbRhSn, and YbNiGa we analyze the effect on the heavy-fermion and magnetic properties of the substitution of Al by isoelectronic In and Ga in YbPtAl and YbNiAl, respectively, and of Ni by Rh in YbNiSn. For this purpose we performed a detailed investigation of the crystallographic (Sec. II) and low-temperature properties (Sec. III) by means of x-ray-diffraction, magnetic susceptibility, magnetization, electrical resistivity, magnetoresistance, thermoelectric-power, and specific-heat measurements. Since our results on the magnetic and transport properties of YbRhSn are in good agreement with those recently published in Refs. 7 and 8, in the present paper we will concentrate on a thermodynamic study of this compound. In the discussion of the results (Sec. IV) we focus on the GS formation of these MO KL's under the influence of strong single-ion anisotropy and frustration of the magnetic interactions.

II. EXPERIMENTAL DETAILS

Polycrystalline samples were prepared by melting appropriate amounts of pure starting elements in closed Ta crucibles, which were previously sealed by arc welding under purified Ar. Heating temperatures of the order of 1650 °C for YbPtIn, 1400 °C for YbRhSn, and 1000 °C for YbNiGa during some minutes were enough to obtain homogeneous samples. After the melting procedure the samples were annealed inside the crucibles at 700 °C for 120 h. X-ray powder-diffraction patterns showed that all samples were single phase. Electron-microprobe analysis revealed neither any evidence of spurious phases (e.g., Yb_2O_3) nor the presence of In, Sn, or Ga within the grain boundaries. YbPtIn and YbRhSn crystallize in the hexagonal ZrNiAl-type structure, whereas YbNiGa in the orthorhombic ϵ-TiNiSi-type structure, as displayed in Table I. Our crystallographic data on YbRhSn are in good agreement with that of previous reports.[7,8,19,20] In the case of the compounds YbPtIn and YbNiGa, single crystals were extracted from the melt and mounted on glass capillary for x-ray analysis. The results of the crystal-structure refinement are detailed in Tables II and III. A single-crystalline rod of YbPtIn of hexagonal cross section (of approximately 3 mm long and 0.8 mm wide) was used for the study of the magnetic and transport properties, as described below. It was confirmed to be oriented with the c axis parallel to the longest axis by means of Laue photographs.

The low-temperature properties of YbPtIn, YbRhSn, and

TABLE II. Crystallographic data for YbPtIn. Structure type: ZrNiAl, space group $P\bar{6}2m$ (No. 189), $Z=3$, $a=0.7548(1)$ nm, $c=0.3766(1)$ nm, $V=0.1888(1)$ nm^3. Intensity data collection and handling: STOE-IPDS, Ag $K\alpha$ radiation ($\lambda=0.560\,86$ Å); 200 exposures, $\Delta\phi=1°$, $2\Theta_{max}=55.63°$, $\mu=553.1$ cm^{-1}; number of reflections: 3929 measured, 371 unique, 360 with $I_{obs}>2\sigma(I_{obs})$; 14 parameters refined; residual values: $R_{gt}(F)=0.019$, $wR(F^2)=0.032$.

Positional and displacement parameters U_{ij} (in 10^{-6} nm^2) for YbPtIn										
Atom	Site	x	y	z	U_{11}	U_{22}	U_{33}	U_{12}	U_{13}	U_{23}
Yb	$3g$	0.4054(1)	0	1/2	77(2)	76(2)	56(2)	38(1)	0	0
In	$3f$	0.7378(1)	0	0	63(2)	65(3)	84(4)	33(1)	0	0
Pt1	$1b$	0	0	1/2	78(2)	U_{11}	70(3)	39(1)	0	0
Pt2	$2c$	2/3	1/3	0	57(1)	U_{11}	78(2)	28(1)	0	0

TABLE III. Crystallographic data for YbNiGa: Structure type: ϵ-TiNiSi, space group $Pnma$ (No. 62), $Z=4$, $a=0.6728(1)$ nm, $b=0.4234(1)$ nm, $c=0.7212(1)$ nm, $V=0.2083(1)$ nm^3. Intensity data collection and handling: STOE-IPDS, Ag $K\alpha$ radiation ($\lambda=0.56086$ Å); 220 exposures, $\Delta\phi=1°$, $2\Theta_{max}=51.34°$, $\mu=350.3$ cm^{-1}. Number of reflections: 3363 measured, 447 unique, 349 with $I_{obs}>2\sigma(I_{obs})$; 20 parameters refined; residual values: $R_{gt}(F)=0.028$, $wR(F^2)=0.056$.

Positional and displacement parameters U_{ij} (in 10^{-6} nm^2) for YbNiGa										
Atom	Site	x	y	z	U_{11}	U_{22}	U_{33}	U_{12}	U_{13}	U_{23}
Yb	4c	0.0124(1)	1/4	0.6976(1)	57(2)	81(2)	76(2)	0	−9(2)	0
Ni	4c	0.2889(2)	1/4	0.4052(2)	99(5)	60(6)	72(7)	0	12(4)	0
Ga	4c	0.1799(2)	1/4	0.0779(2)	93(5)	79(6)	73(7)	0	10(4)	0

YbNiGa were studied using standard experimental techniques. The magnetic susceptibility (χ) and magnetization (M) were measured in a superconducting quantum interference device (SQUID) magnetometer in the temperature range $2<T<400$ K and in magnetic fields up to $B=5.5$ T. The electrical resistivity (ρ) and magnetoresistance were obtained in a commercial physical property measuring system in the range $1.8<T<300$ K and in fields up to 10 T. The thermoelectric power (TEP) was measured on polycrystalline bars down to 2 K using a steady-state method, as described elsewhere.[21] dc electrical-resistivity data were taken simultaneously with the TEP. Additional $\rho(T)$ measurements down to 0.5 K were carried out in a ^{3}He cryostat using the standard four-terminal low-frequency lock-in technique. The specific-heat C_P was measured in a semiadiabatic ^{3}He calorimeter using the heat-pulse method in temperatures $0.5<T<10$ K and in fields up to 8 T.

III. LOW-TEMPERATURE PROPERTIES

A. Magnetic susceptibility and magnetization

In order to eliminate any preferred orientation of the grains in the bulk, the mean value of the magnetic susceptibility and magnetization was measured on random powder, as described elsewhere.[21] This procedure allows us to simulate a measurement on isotropic polycrystalline samples, denoted hereafter χ_{poly} and M_{poly}. The results are displayed in Figs. 1 and 2 for YbPtIn and YbNiGa, respectively. Our data on YbRhSn (not shown here) reproduce the results recently reported in Refs. 7 and 8. The high-temperature magnetic susceptibility $\chi_{poly}(T)$ of the three compounds follows a Curie-Weiss law, with effective magnetic moments close to the value of free Yb^{3+} ($\mu_{eff}=4.5\mu_B$). The respective extrapolated values for the Weiss temperature are $\Theta_P=-30$ K for YbPtIn and YbNiGa and $\Theta_P=-20$ K for YbRhSn. These data are included in a summary of the experimental results in Table IV.

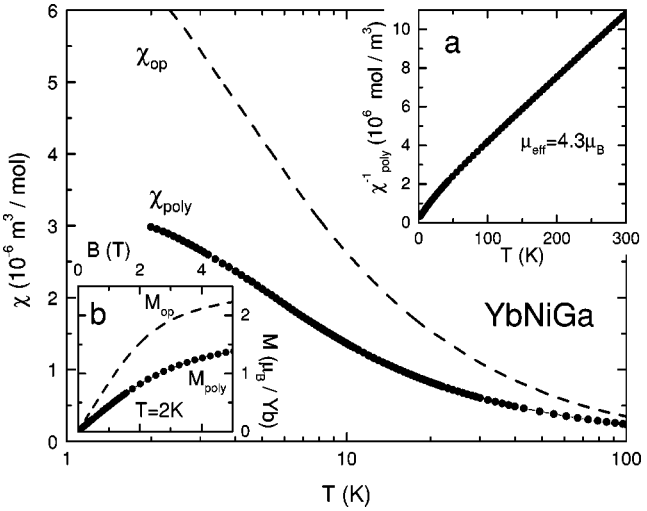

FIG. 2. Magnetic susceptibility of YbNiGa, in a log-T scale, for random powder (χ_{poly}) compared with oriented powder (χ_{op}), as explained in the text. (a) Inverse susceptibility $\chi^{-1}_{poly}(T)$ as a function of temperature. (b) Isothermal magnetization at $T=2$ K for random (M_{poly}) as well as for oriented powder (M_{op}).

At low temperature YbPtIn shows a strong magnetic anisotropy and a weak AFM-like phase transition at 3.5 K (see Fig. 1). The anisotropy of the magnetic properties is investigated by measuring the magnetic susceptibility along the hexagonal basal plane (χ_{aa}) as well as along the c-axis direction (χ_c) of the single crystal. A comparison between the values of χ_{aa} and χ_c provides information about the single-ion anisotropy expected to arise from the local CEF interaction at the Yb site. At low temperatures, the ratio $\chi_{aa}/\chi_c\sim10$ reveals the presence of strong ''easy-plane'' magnetic anisotropy. An analysis of the data along the ''hard'' magnetic direction allows us to observe a broad maximum at $\sim$150 K in χ_c and a large slope of $\chi_c^{-1}(T)$ at low temperature, corresponding to a small effective magnetic-moment of the GS doublet along this direction [see Fig. 1(b)]. This behavior is characteristic of magnetic systems with low-CEF symmetry and large anisotropy, in which a maximum in the susceptibility is expected to be present along the hard magnetic direction, whereas the susceptibility along the easy (and eventually intermediate) axis rises monotonously upon low-

TABLE IV. Summary of the experimental data of YbPtIn, YbRhSn, and YbNiGa: high-temperature effective magnetic moment μ_{eff} [μ_B/Yb], extrapolated Weiss temperature Θ_P [K], magnetic ordering temperatures T_{N1}, T_{N2} [K], temperature of the maximum of the electrical resistivity $T_{max,\rho}$ [K], of the minimum of the Seebeck coefficient $T_{min,TEP}$ [K], extrapolated γ_o coefficient [mJ/mol K^2] and entropy gain ΔS [Rln2], as described in the text.

	μ_{eff}	Θ_P	T_{N1}, T_{N2}	$T_{max,\rho}$	$T_{min,TEP}$	γ_o	ΔS
YbPtIn	4.4	−30	3.4, 1.4	3.5	4, 160	430	0.6
YbRhSn	4.3	−20	1.85, 1.4	4.5		360	0.7
YbNiGa	4.4	−30	1.9, 1.7	4.2		450	0.5

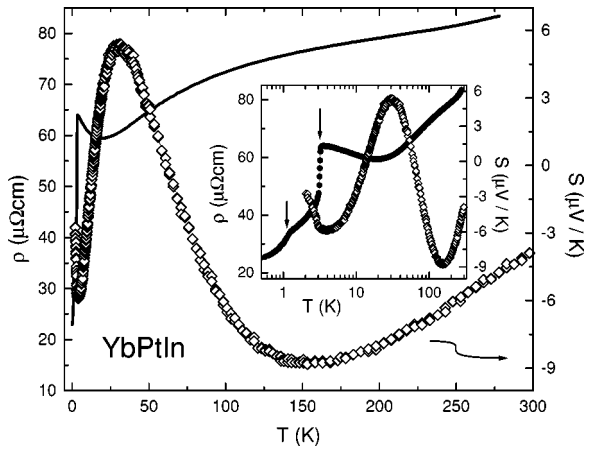

FIG. 3. Temperature dependence of the electrical resistivity (ρ) and the thermoelectric power (TEP) of YbPtIn measured on a polycrystalline sample. Inset: ρ and TEP data on a logarithmic scale. The arrows indicate the temperature of the magnetic transitions as described in the text.

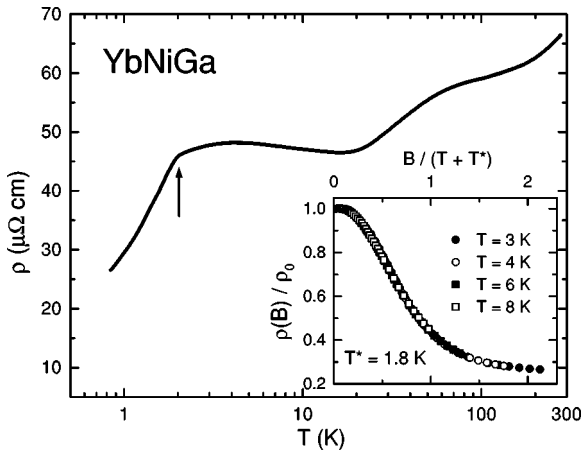

FIG. 4. Electrical resistivity of YbNiGa as ρ vs T (on a logarithmic scale). The arrow points to the magnetic transition at $T_{N1}=1.9$ K. Inset: magnetoresistance plotted as $\rho(B)/\rho(0)$ versus $B/(T+T^*)$, with $T^*=1.8$ K, in the temperature range $3\leqslant T\leqslant 8$ K.

ering the temperature.[22] Since the susceptibility of the latter (i.e., χ_{aa} in our case) is much larger than that along the hard axis (i.e., χ_c), the weighted sum over all directions in $\chi_{poly}(T)$ shows only slight evidence of the CEF effects, as observed in Fig. 1(b). The strong anisotropic magnetic response of YbPtIn is also present in the low-temperature magnetization as well. $M(B)$ data measured at $T=2$ K along both directions (M_{aa} and M_c) are compared with data taken on random powder (M_{poly}) in Fig. 1(c), showing that the strong magnetocrystalline anisotropy survives up to large fields. The weakness of the magnetic transition of YbPtIn might be an indication of the presence of geometrically frustrated magnetic interactions, as discussed below.

Regarding YbNiGa and YbRhSn, no indication of MO is found down to 2 K. Nevertheless the influence of the single-ion anisotropy on the magnetic properties can be studied by comparing $\chi_{poly}(T)$ and $M_{poly}(B)$ with measurements made on oriented powder, denoted by χ_{op} and M_{op}, respectively. The latter allows one to simulate a measurement along the easy magnetic direction, as confirmed for YbPtIn, for which $\chi_{op}\simeq\chi_{aa}$ and $M_{op}\simeq M_{aa}$. The $\chi_{op}(T)$ and $M_{op}(B)$ data of YbNiGa are included as a dashed-line in Fig. 2, where the ratio χ_{op}/χ_{poly} reaches a factor of more than 2 at low temperatures. According to this result the single-ion anisotropy in YbNiGa should be of easy-axis type, since for an easy-axis paramagnet one expects $1<\chi_{op}/\chi_{poly}<3$, whereas $1<\chi_{op}/\chi_{poly}<3/2$ is expected for easy-plane anisotropy.[21] The same easy-axis-type anisotropy ratio is manifested in the low-temperature magnetization of YbNiGa [see Fig. 2(b)]. Concerning YbRhSn, the ratio $\chi_{op}/\chi_{poly}\simeq 1.3$ is comparable to that observed for YbPtIn between χ_{aa} and χ_{poly} [see Fig. 1(a)]. This analysis suggests that the magnetic anisotropy is of easy-plane type for the hexagonal compounds YbPtIn and YbRhSn, whereas it is of easy-axis type for orthorhombic YbNiGa.

B. Electrical resistivity and thermoelectric power

The electrical resistivity data of YbPtIn and YbNiGa are plotted in Figs. 3 and 4. In both cases $\rho(T)$ decreases slowly with decreasing temperature, showing a broad shoulder centered at around 100 K and a minimum at ~ 20 K. Below this temperature $\rho(T)$ increases as $-\ln T$ upon decreasing the temperature, followed by a maximum at $T_{max,\rho}\sim 4$ K and a steep decrease below 3.4 K for YbPtIn and 1.9 K for YbNiGa, signaling the onset of MO. At lower temperatures, a further anomaly is present in YbPtIn at around 1.3 K (see inset of Fig. 3). In contrast, our $\rho(T)$ data on YbRhSn (not shown here) diminishes almost linearly as T decreases. Below 10 K, a weak logarithmic increase is followed by a maximum at $T_{max,\rho}\sim 4.5$ K (see Ref. 7). Two magnetic transitions are also present at 1.85 and 1.4 K in YbRhSn, respectively, as discussed below.

The effect of the magnetic field on the low-temperature electrical resistivity of YbPtIn is displayed in Fig. 5(a), where $\rho(T)$ is measured along the c axis of the single crystal, while $B\leqslant 10$ T is applied parallel to the hexagonal basal

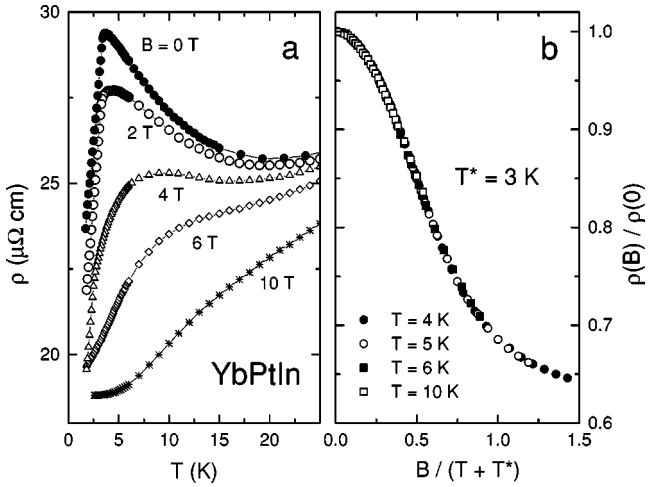

FIG. 5. (a) Low-temperature electrical resistivity of a single crystal of YbPtIn, as ρ vs T, measured along the c axis for different fields $B\leqslant 10$ T applied along the hexagonal basal plane. (b) Magnetoresistance plotted as $\rho(B)/\rho(0)$ versus $B/(T+T^*)$, with $T^*=3$ K, in the temperature range $4\leqslant T\leqslant 10$ K.

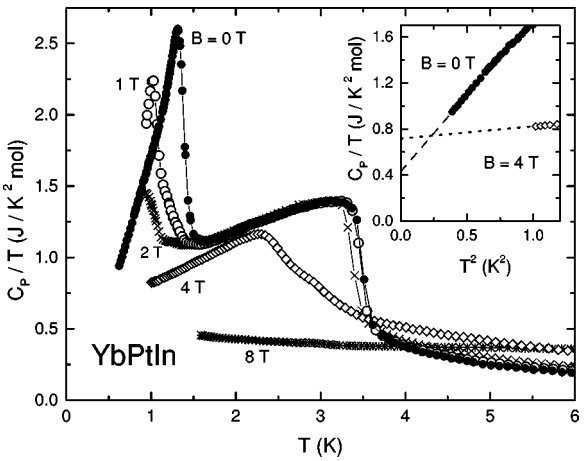

FIG. 6. Low-temperature specific heat of YbPtIn as C_P/T vs T, for $B \leqslant 8$ T. Inset: low-temperature data plotted as C_P/T vs T^2. Dashed lines are guide to the eye.

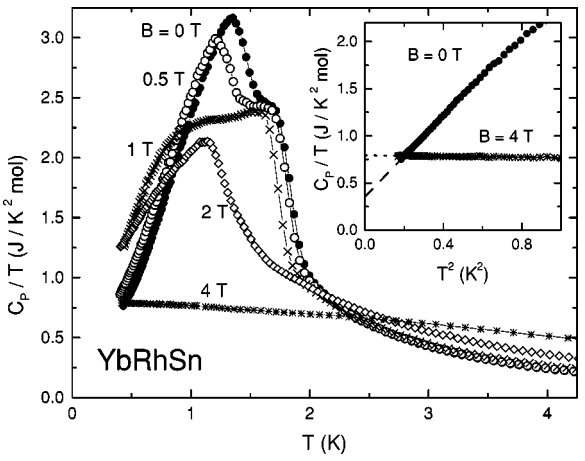

FIG. 7. Low-temperature specific heat of YbRhSn as C_P/T vs T, for $B \leqslant 4$ T. Inset: low-temperature data plotted as C_P/T vs T^2. Dashed lines are guides to the eye.

plane. Whereas the Kondo scattering is gradually suppressed upon increasing the field, the signatures of the MO remain almost unaffected up to $B \simeq 4$ T. Above the ordering temperature $\rho(B)-\rho(0)$ is always negative, suggesting a description in terms of a single-ion Kondo model. In fact, Fig. 5(b) shows that the normalized magnetoresistance $\rho(B)/\rho(0)$ can be scaled when plotted as a function of $B/(T+T^*)$, T^* being a measure of the Kondo temperature. This scaling law is predicted in the Bethe Ansatz solution to the Coqblin-Schrieffer model[23] and has been proven to describe quantitatively magnetoresistance results of some KL systems.[4,24,25] A similar scaling behavior is also possible for polycrystalline samples of YbNiGa, as shown in the inset of Fig. 4, indicating that the underlying physics of these compounds is dominated by a single energy scale related to the Kondo temperature.

In order to obtain more information about the influence of the Kondo effect on the GS properties of these compounds, TEP is measured on a polycrystalline sample of YbPtIn (see Fig. 3). In general, the TEP of heavy-fermion compounds is characterized by showing much larger values than normal metals as a consequence of the enhancement of the density of electronic states at the Fermi energy. The TEP of YbPtIn reaches -9 μV/K at the minimum present at ~ 150 K and -6 μV/K at the low-temperature minimum at $T_{\mathrm{min,TEP}} \sim 4$ K. A strong upward deviation occurs below 3.4 K in coincidence with the steep decrease observed in $\rho(T)$ (see inset of Fig. 3). This TEP curve is symmetrically similar (with inverted signs) to those of archetypal Ce-based KL systems, like $CeRu_2Si_2$,[26] reflecting the hole-electron analogy of the Yb-4f^{13} and Ce-4f^1 configurations.[3,26]

C. Specific heat

The low-temperature specific-heat data of YbPtIn, YbRhSn, and YbNiGa are plotted as C_P/T vs T in Figs. 6, 7, and 8, respectively. For the three compounds double magnetic transitions are observed at $T_{N1}=3.4$ K and $T_{N2}=1.4$ K for YbPtIn, at $T_{N1}=1.85$ K and $T_{N2}=1.4$ K for YbRhSn, and at $T_{N1}=1.9$ K and $T_{N2}=1.7$ K in YbNiGa (Ref. 42) (see Table IV). In applied magnetic field these anomalies shift to lower temperatures, as expected for AFM transitions. In the case of YbPtIn and YbRhSn (Figs. 6 and 7) the transitions at T_{N1} and T_{N2} gradually disappear and evolve into flat, enhanced C_P/T values for $B>4$ T. The strong changes in the C_P data of these compounds between $B=2$ T and $B=4$ T are probably related to the evolution from a field-induced canted AFM-like spin arrangement at 2 T to a field-induced ferromagnetic like spin arrangement at 4 T. This can be deduced from the $M(B)$ curve showing an almost linear slope between $B=0$ T and $B \sim 2$ T, but being nearly saturated at $B=4$ T [Fig. 1(c)]. The $\rho(T,B)$ data also present strong changes for B slightly larger than 4 T [Fig. 5(a)].

In view of the AFM nature of these magnetic transitions, the C_P temperature dependence below 1 K can be described in all cases as $C_P/T=\gamma_o+DT^2$, corresponding to the expected dispersion relation of AFM magnons, as shown in the insets of Figs. 6, 7, and 8. The extrapolated values of γ_o are 430 mJ/mol K^2 for YbPtIn, 360 mJ/mol K^2 for YbRhSn, and 450 mJ/mol K^2 for YbNiGa, being among the highest γ_o values of known Yb-based intermetallics,[2] as discussed below. The entropy gain ΔS, calculated by integrating $C_P(T)/T$ up to the highest transition temperature amounts to

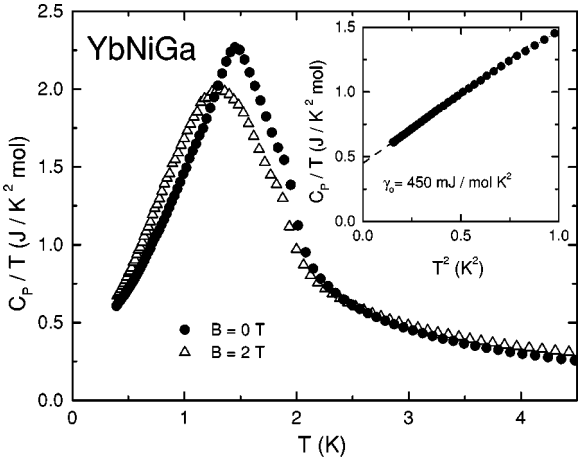

FIG. 8. Low-temperature specific heat of YbNiGa as C_P/T vs T, for $B=0$, and 2 T. Inset: low-temperature data plotted as C_P/T vs T^2. Line is a guide to the eye.

60% for YbPtIn, 70% for YbRhSn, and to 50% for YbNiGa of the expected value $R\ln 2$ for a GS doublet (see Table IV). In this procedure we neglect the contribution of the phononic term to the total C_P. Since the shape of the $C_P(T)$ curves does not show indications of strong magnetic correlations above T_{N1}, a large part of the entropy reduction has to be attributed to the presence of the Kondo effect.

IV. DISCUSSION AND CONCLUSIONS

In the compounds YbPtIn, YbRhSn, and YbNiGa the competition between Kondo and RKKY interactions leads to the formation of a MO heavy-fermion GS which, in comparison to the situation of Ce systems, is rarely observed in Yb-based intermetallics.[2] In addition, they present interesting magnetic properties as well. In the following we discuss the main features of these compounds focusing on two main aspects: their heavy-fermion behavior and the influence on the GS properties of strong single-ion anisotropy and frustration of the magnetic interactions.

The transport properties of YbPtIn, YbRhSn, and YbNiGa resemble the characteristic features observed in several Ce-based KL's, namely the presence of Kondo effect in $\rho(T)$ and enhanced values of the TEP like in, e.g., $CeCu_2Ge_2$.[4,27] The $\rho(T)$ data of YbPtIn and YbNiGa show broad anomalies at $\sim$150 K which are due to the interaction of Kondo-type incoherent scattering on excited CEF levels[28] (see also Sec. III A). At lower temperatures the $\rho(T) \propto -\ln T$ dependence, present in different degree of intensity in the three compounds[7] and followed by a clear maximum at $T_{\max,\rho}$, signals the effect of incoherence Kondo scattering on the GS doublet. In YbPtIn, $T_{\max,\rho}$ coincides with the minimum of TEP at $T_{\min,\mathrm{TEP}} \sim 4$ K, where the magnitude of the TEP is at least a factor of 2 larger than that of, e.g., the heavy-fermion compound YbNiSn.[29] For YbPtIn as well as for YbNiGa, the value of $T_{\max,\rho}$ agrees with the value of the Kondo temperature extracted from the scaling behavior of the magnetoresistivity data.

The presence of Kondo effect is also manifested in the C_P results as well. The enhanced values of the Sommerfeld coefficient $\gamma_o > 350$ mJ/mol K^2 (see Table IV) are among the largest observed so far for Yb-based MO KL's. Correspondingly, due to Kondo compensation the entropy gain is as low as 50% of the expected value $R\ln 2$. In contrast to the case of Ce-based heavy fermions, where γ_o values larger than 400 mJ/mol K^2 are typical,[4] this is not the case of Yb systems.[2] Some of the very few exceptions of *atomically ordered* intermetallic compounds with $\gamma_o > 350$ mJ/mol K^2 are: YbPdBi (470 mJ/mol K^2),[30] YbSi (500 mJ/mol K^2),[31] $YbNi_2B_2C$ (530 mJ/mol K^2),[32] YbPd (600 mJ/mol K^2),[33] Yb_2Ni_2Al (700 mJ/mol K^2),[34] and YbBiPt (8000 mJ/mol K^2).[35] In particular, the YbTX compounds of the present study also show enhanced γ_o values in comparison to the orthorhombic compounds YbPtAl (200 mJ/mol K^2) (Ref. 13) and YbNiSn (300 mJ/mol K^2),[36] and to the hexagonal compound YbNiAl (350 mJ/mol K^2) (Ref. 13) (cf. Table IV). The substitution of X=Al by isoelectronic X=In and Ga in YbPtIn and YbNiGa, respectively, as well as T=Ni by Rh in YbRhSn produces in all cases a change of the crystallographic structure, from orthorhombic ϵ-TiNiSi to hexagonal ZrNiAl-type structure and vice versa. In YbPtIn and YbNiGa this effect changes the environmental distribution of the ligands around Yb leading to an enhancement of the density of states at the Fermi level. As a consequence γ_o increases in more than a factor of 2 in YbPtIn with respect to YbPtAl and up to 450 mJ/mol K^2 in YbNiGa. In the case of YbRhSn, the situation is, however, different due to the involved change in the electronic structure. Since the substitution of T=Ni by Pd leads to MV behavior in (ϵ-TiNiSi-type) YbPdSn,[37] the change to T=Rh with one d hole more in its electronic configuration is expected to stabilize the Yb^{3+} configuration with respect to the almost divalent one in YbPdSn.[37] As a result, MO and $\gamma_o = 360$ mJ/mol K^2 are observed in YbRhSn.

Concerning the magnetic properties of YbPtIn, YbRhSn, and YbNiGa, they evidence the competition between strong single-ion anisotropy and frustration of the magnetic interactions. Whereas the strong magnetic anisotropy is a consequence of CEF effects acting on the R-crystallographic site, the frustration of the magnetic interactions is directly related to the topology of the underlying crystal structure. Therefore in these KL compounds, besides the competition between Kondo and RKKY interactions, these additional mechanisms should be taken into account in the analysis of the GS properties.

In the hexagonal compound YbPtIn strong CEF effects force the magnetic moments to adopt an easy-plane configuration (see Fig. 1). Our analysis of the magnetic properties of YbRhSn using random and oriented powder suggest a similar magnetic anisotropy for this hexagonal compound as well. In addition to strong magnetocrystalline anisotropy, the presence of AFM coupling between magnetic moments sitting in a hexagonal coordination-symmetry should lead to a geometrical frustration of the exchange interactions. Since there is only one equivalent crystallographic site for the Yb moments in these structures, the second magnetic transition at T_{N2} can be considered as an evidence of the difficulty of the spin system to find an arrangement in order to minimize its free energy. Furthermore, an induced ferromagnetic alignment of the moments is reached in a relatively low magnetic field ($B \sim 5$) T, pointing to a weak, frustrated AFM coupling. This is corroborated by very recent neutron-diffraction experiments that reveal the presence of complex and incommensurate magnetic structures in both compounds.[38] The behavior of YbPtIn and YbRhSn resembles that of UNi_4B: another hexagonal compound in which the f moments lie along the basal plane of the structure. Despite the sharp AFM phase transition at $T_N = 20$ K, 1/3 of the magnetic moments remain frustrated (i.e., paramagnetic) down to low temperature,[39,40] until a second magnetic transition takes place at 330 mK.[41] Hence YbPtIn and YbRhSn are candidates for further microscopic studies of the effect of geometrical frustration in an easy-plane AFM hexagonal KL.

For the orthorhombic compound YbNiGa the incipient onset of MO at 1.9 K seems to be replaced by another magnetic transition occurring at 1.7 K as observed in the C_P data of Fig. 8.[42] This situation resembles the multiple magnetic phase transitions present in orthorhombic YbPtAl,[13] attributed to competing CEF effects and frustrated anisotropic exchange interactions between nearest and next-nearest (crystallographically equivalent) Yb neighbors sitting zigzag

chains perpendicular to each other.[15] Preliminary neutron-diffraction results on YbNiGa,[38] as well as on YbPtAl,[43] indicate also incommensurate and therefore complex magnetic structures. Since such experiments on powder have been so far unsuccessful to unambiguously determine the magnetic structures, experiments on single crystals are indispensable, project which is currently under way.

As a conclusion, the low-temperature properties of YbPtIn, YbRhSn, and YbNiGa show the archetypal properties of MO KL's. The presence of Yb^{3+} moments at room temperature, the logarithmic increase in $\rho(T)$, the enhanced TEP, the scaling behavior of the magnetoresistance, the reduced entropy gain at the ordering temperature, and the γ_o values as large as 450 mJ/mol K^2 clearly identify these compounds as heavy-fermion AFM-systems. These results reveal a systematic enhancement of the density of state at the Fermi level with respect to the (isoelectronic) homologues YbPtAl, YbNiSn, and YbNiAl. The magnetic properties show strong single-ion anisotropy induced by CEF effects which compete with frustrated magnetic interactions due to the topology of the underlying structure. This competition leads to double magnetic transitions and suggests the presence of complex magnetic structures in a similar situation to other *f*-electron compounds.

Note added. While preparing this manuscript, we learned that D. Kaczorowski *et al.* have performed an independent study on YbPtIn.

ACKNOWLEDGMENTS

We are grateful to Zakir Hossain, Arno Hiess, Georg Ehlers, J. P. Sanchez, and D. Kaczorowski for valuable conversations. One of us (O.T.) acknowledges the Alexander von Humboldt Foundation for its support.

[1] N.D. Mathur, F.M. Grosche, S.R. Julian, I.R. Walker, D.M. Freye, R.K.W. Haselwimmer, and G.G. Lonzarich, Nature (London) **394**, 39 (1998), and references therein.

[2] Z. Fisk and M. B. Maple, J. Alloys Compd. **183**, 303 (1992).

[3] J. D. Thompson and J. L. Lawrence, in *Handbook on the Physics and Chemistry of the Rare Earths*, edited by K. A. Gschneidner, Jr., L. Eyring, G.H. Lander, and G.R. Choppin (North-Holland, Amsterdam, 1994), Vol. 19, p. 383.

[4] N. Grewe and F. Steglich, in *Handbook on the Physics and Chemistry of the Rare Earths*, edited by K. A. Gschneidner, Jr., and L. Eyring (North-Holland, Amsterdam, 1991), Vol. 14, p. 343.

[5] S. Doniach, in *Valence Instabilities and Related Narrow Band Phenomena*, edited by R.D. Parks (Plenum, New York, 1977), p. 169; Physica B & C **91B**, 231 (1977); J.R. Iglesias, C. Lacroix, and B. Coqblin, Phys. Rev. B **56**, 11 820 (1997).

[6] K. Katoh, T. Takabatake, A. Minami, I. Oguro, and H. Sawa, J. Alloys Compd. **261**, 32 (1997).

[7] D. Kaczorowski, A. Leither-Jasper, P. Rogl, H. Flandorfer, T. Cichorek, R. Pietri, and B. Andraka, Phys. Rev. B **60**, 422 (1999).

[8] K. Katoh, G. Terui, Y. Niide, H. Aoki, and A. Ochiai, Physica B **259-261**, 161 (1999).

[9] T. Suzuki, Y. Matsumoto, F. Masaki, K. Izawa, M. Ito, K. Kaoh, T. Takabatake, and T. Fujita, Physica B **259-261**, 146 (1999).

[10] P. Villars and L. D. Calvert, *Pearson's Handbook of Crystallographic Data for Intermetallic Phases* (ASM, Materials Park, OH, 1991), 2nd ed.

[11] E. Parthé and B. Chabot, in *Handbook on the Physics and Chemistry of the Rare Earths*, edited by K. A. Gschneidner, Jr., and L. Eyring (North-Holland, Amsterdam, 1984), Vol. 6, p. 113.

[12] See, for instance, V. Sechovsky and L. Havela, in *Ferromagnetic Materials*, edited by E. P. Wohlfarth and K.H.J. Buschow (North-Holland, Amsterdam, 1988), Vol. 4, p. 309.

[13] C. Schank, G. Olesch, J. Köhler, U. Tegel, U. Klinger, J. Diehl, S. Klimm, G. Sparn, S. Horn, C. Geibel, and F. Steglich, J. Magn. Magn. Mater. **140&144**, 1237 (1995).

[14] K. Drescher, M.M. Abd-Elmeguid, H. Micklitz, J.P. Sanchez, C. Geibel, and F. Steglich, J. Magn. Magn. Mater. **182**, L275 (1998).

[15] K. Drescher, M.M. Abd-Elmeguid, H. Micklitz, and J.P. Sanchez, Phys. Rev. Lett. **77**, 3228 (1996), and references therein.

[16] G. Ehlers, C. Geibel, F. Steglich, and H. Maletta, Z. Phys. B: Condens. Matter **104**, 393 (1997).

[17] A. Dönni, G. Ehlers, H. Maletta, P. Fischer, H. Kitazawa, and M. Zolliker, J. Phys.: Condens. Matter **8**, 11 213 (1996).

[18] G. Ehlers and H. Maletta, Z. Phys. B: Condens. Matter **101**, 317 (1996).

[19] A.E. Dwight, W.C. Harper, and C.W. Kimball, J. Less-Common Met. **30**, 1 (1971).

[20] E. I. Gladyshevsky, O. I. Bodak, and V. K. Pecharsky, in *Handbook on the Physics and Chemistry of the Rare Earths*, edited by K. A. Gschneidner, Jr., and L. Eyring (North-Holland, Amsterdam, 1990), Vol. 13, p. 1.

[21] O. Trovarelli, C. Geibel, B. Buschinger, R. Borth, S. Mederle, M. Grosche, G. Sparn, and F. Steglich, Phys. Rev. B **60**, 1136 (1999).

[22] See, for example, K. Katoh, A. Ochiai, and T. Suzuki, Physica B **223&224**, 340 (1996).

[23] P. Schlottmann, Z. Phys. B: Condens. Matter **51**, 223 (1983).

[24] D.T. Adroja, B.D. Rainford, and A.J. Neville, Physica B **223&224**, 279 (1996).

[25] J. Diehl, H. Davideit, S. Klimm, U. Tegel, C. Geibel, F. Steglich, and S. Horn, Physica B **206&207**, 344 (1995).

[26] D. Jaccard and J. Sierro, in *Valence Instabilities*, edited by P. Wachter and H. Boppart (North-Holland, Amsterdam, 1982), p. 409.

[27] D. Jaccard, K. Behnia, and J. Sierro, Phys. Lett. A **163**, 475 (1992).

[28] D. Cornut and B. Coqblin, Phys. Rev. B **5**, 4541 (1972).

[29] K. Alami-Yadri and D. Jaccard, J. Low Temp. Phys. **114**, 135 (1998).

[30] S.K. Dahr, N. Nambudripad, and R. Vijayaraghavan, J. Phys. F: Met. Phys. **18**, L41 (1988).

[31] C. Engkagul, R. Selim, T. Mihalisin, and P. Schlottmann, Phys. Rev. B **35**, 3686 (1987).

[32] A. Yatskar, N.K. Budraa, W.P. Beyermann, P.C. Canfield, and S.L. Bud'ko, Phys. Rev. B **54**, 3772 (1996).

[33] R. Pott, W. Boksch, G. Leson, B. Politt, H. Schmidt, A. Freimuth, K. Keulerz, J. Langen, G. Neumann, F. Oster, J. Röhler, U.

Walter, P. Weidner, and D. Wohlleben, Phys. Rev. Lett. **54**, 481 (1985).
[34] C. Geibel, U. Klinger, B. Buschinger, M. Weiden, G. Olesch, F. Thomas, and F. Steglich, Physica B **223&224**, 370 (1996).
[35] Z. Fisk, P.C. Canfield, W.P. Beyermann, J.D. Thompson, M.F. Hundley, H.R. Ott, E. Felder, M.B. Maple, M.A. Lopez de la Torre, P. Visani, and C.L. Seaman, Phys. Rev. Lett. **23**, 3310 (1991).
[36] M. Kasaya, T. Tani, K. Kawate, T. Mizushima, Y. Isikawa, and K. Sato, J. Phys. Soc. Jpn. **61**, 2209 (1992).
[37] D.T. Adroja and S.K. Malik, Phys. Rev. B **45**, 779 (1992).
[38] G. Ehlers (private communication).
[39] J.A. Mydosh, Z. Phys. B: Condens. Matter **103**, 251 (1997), and references therein.
[40] S.A.M. Mentink, G.J. Nieuwenhuys, A.A. Menovsky, J.A. Mydosh, A. Drost, and E. Frikkee, Physica B **206-207**, 473 (1995).
[41] R. Movshovich, M. Jaime, S. Mentink, A.A. Menovsky, and J.A. Mydosh, Phys. Rev. Lett. **83**, 2065 (1999).
[42] The value of the transition temperatures $T_{N1}=1.9$ K and $T_{N2}=1.7$ K are extracted from the minima in the derivative dC_P/dT at $B=0$.
[43] J. P. Sanchez (private communication).